



## MODELING AND ANALYSIS OF A NONLINEAR PIEZOAEROELASTIC WING

Wander Gustavo Rocha Vieira<sup>1</sup>

Carlos De Marqui Jr.<sup>2</sup>

Department of Aeronautical Engineering, EESC-USP, São Carlos, SP, Brasil  
wandergrv@gmail<sup>1</sup>, demarqui@sc.usp.br<sup>2</sup>

**Abstract.** For the past years, there has been an increase in research in the area of vibration based energy harvesting. The main motivation is to provide electrical energy for remotely operated systems with limited energy sources. Different transduction mechanisms can be used for vibration to electricity conversion. However, the piezoelectric one has received the most attention due to the ease of use and power density it provides. Although aeroelastic phenomena are usually avoided, the conversion of aeroelastic vibrations into electrical energy is a powerful option for wind energy harvesting. In this work the main goal is the investigation of the interaction of piezoelectric energy harvesting and a nonlinear aeroelastic plate. The interaction of piezoelectric energy harvesting and the nonlinear behavior can have interesting aspects for energy conversion using limit cycle oscillation (LCO). An electromechanically coupled nonlinear finite element model is presented. The von Karman large deflection strain-displacement relations will be considered. Roger's approximation will be used to obtain the unsteady aerodynamic loads. In the electrical domain, a resistive load is considered. The numerical time-domain equations are solved using the alpha generalized method and a Newton Raphson procedure. This work presents the effect of varying the aspect ratio (1,2,3,4 and 5) not only for linear flutter speed but also for the mechanical and electrical outputs obtained after the linear flutter speed. First, the results show that the increasing of the aspect ratio decreases the linear flutter speed. Then, this work discusses the behavior of mechanical (displacement) and electrical (voltage and powered) variables obtained after the flutter speed for different aspect ratio and resistive loads.

**Keywords:** energy harvesting, flutter, piezoelectric, aeroelasticity

### 1. INTRODUCTION

The transformation of aeroelastic vibrations into electrical energy has received growing attention in the last few years. The goal is to convert flow-induced structural vibrations into electricity by using aeroelastic systems with electromechanical coupling. The harvested energy can be used to power small electronic components. Although different transduction mechanisms can be used for vibration-to-electricity conversion, such as the piezoelectric, electromagnetic, and electrostatic transductions [1], the recent papers have focused on the piezoelectric transduction [2-5] due to the ease of application and high power density of piezoelectric materials. The power extraction from linear and nonlinear aeroelastic systems has been covered in the literature. An early experimental effort of generating electricity from thin curved airfoils with macro-fiber composite (MFC) piezoelectric structures under airflow excitation was presented by Erturk et al. [6]. For the piezoaeroelastic problem of harvesting energy from airflow excitation of a cantilevered plate with embedded piezoceramics, De Marqui et al. [7,8] presented linear finite element models based on the vortex-lattice method [18] and the doublet-lattice method [8] of aeroelasticity [9-12]. Time domain simulations [7] were given for a cantilevered plate with embedded piezoceramics for various airflow speeds below the linear flutter speed and at the flutter boundary. Frequency domain simulations [8] considering resistive and resistive inductive circuits were also presented focusing on the linear response at the flutter boundary. Bryant and Garcia [13,14] studied the aeroelastic energy harvesting problem for a typical section by using the finite state theory of Peters et al. [15]. Erturk et al. [16] presented an experimentally validated lumped-parameter model for an airfoil with piezoceramics attached onto plunge stiffness members using Theodorsen's [17] aerodynamic model. Piezoelectric power generation at the flutter boundary, including the minor shift in the linear flutter speed has also been discussed [16]. In addition to these recent efforts, the "wingmill" concept was investigated previously for rather large-scale configurations as an alternative to conventional windmills and wind turbines [18-20].

A linear aeroelastic system undergoing persistent oscillations at the neutral stability condition (i.e. at the linear flutter speed) is the ideal linear scenario [7,16]. However, persistent oscillations occurring at a specific wind speed restrict the operating envelope of the energy harvester and often inherent nonlinearities are present. Nonlinear systems present a very rich variety of dynamic behavior such as LCOs, internal resonances, and chaotic motion [21,22]. In Erturk et al. [16], the possible useful consequences of having nonlinearities in the system to create limit-cycle oscillations (LCOs) in aeroelastic harvesters was first discussed. More recently, researchers have focused on nonlinear aspects [23] of aeroelastic energy harvesting using piezoelectric transduction and airfoil configurations. Abdelkefi et al. [24] considered nonlinear plunge and pitch stiffness components (in polynomial forms) and theoretically investigated

their effects on the harvested energy and the nonlinear aeroelastic behavior. Sousa et al. [25] considered free play nonlinearity for the pitch stiffness and experimentally validated its effect on the harvested piezoelectric energy. The case of combined nonlinearities (free play and cubic hardening stiffness) was also numerically investigated by the same authors [25]. The free play nonlinearity has been shown to reduce the cut-in speed of persistent oscillations while the hardening stiffness of the cubic form has been observed to make the persistent oscillations bounded at acceptable amplitudes over a wide range of airflow speeds.

The literature of aeroelastic energy harvesting has covered the linear modeling and analysis of plate-like wings for low power generation [7,8]. In this paper, wing-like configurations are investigated for low-power generation from nonlinear aeroelastic oscillations in unmanned aerial vehicle (UAV) applications. An electromechanically coupled finite element model based on von Karman plate assumptions is combined with an unsteady Doublet-lattice (originally in frequency domain) aerodynamic model. The aerodynamic model is later converted to the time domain by using Roger's approximation[26]. A load resistance is considered in the electrical domain of the problem. The set of nonlinear equations is solved with the iterative Newton-Raphson method and the generalized alpha method. Five wing configurations with different aspect ratios are investigated. The effect of the aspect ratio on the linear aeroelastic behavior is first investigated for the short circuit condition. Later, the nonlinear electroaeroelastic behavior is investigated for a range of load resistances and the different aspect ratios of the linear case. The effects of aspect ratio and load resistance on the cut-in speed of limit cycle oscillations (LCOs), on the range of airflow speeds of LCOs of acceptable amplitudes and on the mechanical and electrical outputs are investigated.

## 2. NON LINEAR PIEZOAEROELASTIC MODEL

This section presents the nonlinear modeling of the electromechanically coupled plate like wing shown in Figure 1. The substructure and the piezoceramic layers are assumed to be perfectly bonded to each other. The piezoceramic layers are poled in the thickness direction and covered by continuous electrodes (which are assumed to be perfectly conductive) with negligible thickness. A resistive load will be considered in the electrical domain and the purpose is to estimate the power generated in the electrical domain due to the nonlinear aeroelastic vibrations of the energy harvester wing as well as the influence of electrical power generation on the nonlinear aeroelastic behavior of the wing.

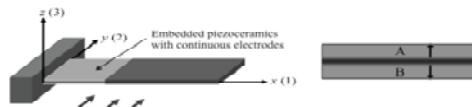


Figure 1- Cantilevered plate like wing with embedded piezoceramic layers and the cross-sectional view.

The electroaeroelastic model is obtained by combining an electromechanically coupled finite element model and an unsteady aerodynamic model. The nonlinear electromechanically coupled model of the wing with embedded piezoceramics is based on von Karman nonlinear relations using classical plate theory [27]. The generalized Hamilton's principle for a piezoelectric energy harvester is used with a finite element (FE) procedure that accounts for the piezoelectric effect and the nonlinear compatibility equation. The electromechanical coupling is included in the constitutive equation that is written in terms of the classical laminate plate theory due the composite nature of the plate. The compatibility equation represents a nonlinear relation between the strain and transversal displacement in order to represent large transversal displacement of the wing. A detailed derivation of the FE model as well as the derivation of the element matrices can be found in references [27,28]. The unsteady aerodynamic model uses the doublet-lattice method (DLM) and the Roger's method [26].

The governing equations of the nonlinear electromechanically coupled plate are presented as,

$$\bar{\mathbf{M}}\ddot{\boldsymbol{\eta}} + \bar{\mathbf{K}}\boldsymbol{\eta} - \bar{\boldsymbol{\Theta}}_2 V_p + \mathbf{K}_{2nl}(\boldsymbol{\eta}, \boldsymbol{\eta})\boldsymbol{\eta} = \mathbf{F} \quad (1.a)$$

$$C_p \dot{V}_p + \bar{\boldsymbol{\Theta}}_2 \dot{\boldsymbol{\eta}} + \frac{1}{R_L} V_p = 0 \quad (1.b)$$

where  $\bar{\mathbf{M}}$  is the modal matrix,  $\bar{\mathbf{K}}$  is the linear stiffness matrix,  $\bar{\boldsymbol{\Theta}}_2$  is the electromechanical coupling vector,  $\bar{\mathbf{F}}_w$  is the external force vector,  $\boldsymbol{\eta}$  is the vector of modal amplitudes,  $C_p$  is the equivalent capacitance,  $V_p$  is the electrical voltage and  $R_L$  is the resistive load. The formulation presented in this work has constant nonlinear stiffness matrix ( $\mathbf{K}_{2nl}(\boldsymbol{\eta}, \boldsymbol{\eta})$ ) [28]. Therefore, the updating is not required during the simulation steps. The nonlinear stiffness matrix ( $\mathbf{K}_{2nl}(\boldsymbol{\eta}, \boldsymbol{\eta})$ ), originally presented by Lee et al. [28], is expressed as the sum of products of the modal coordinates and nonlinear stiffness matrices:

$$\mathbf{K}_{nl2} = \sum_{i=1}^n \sum_{k=1}^n \eta_i \eta_k \mathbf{K}_{nl2}^{ik}(\boldsymbol{\Phi}_i, \boldsymbol{\Phi}_k) \quad (2)$$

where the subscripts i and k are related to the ith and kth modes.

In this work, the right-hand-side term F of the mechanical equation (Eq. 1a) is the vector of unsteady aerodynamic loads obtained from the unsteady DLM. In this method, the linearized formulation for the oscillatory, inviscid, subsonic lifting surface theory relates the normal velocity at the surface of a body (e.g., an elastic wing) with the aerodynamic loads caused by the pressure distribution [29]. The formulation is derived using the unsteady Euler equations of the surrounding fluid. The doublet singularity (or a sheet of doublets) is a solution of the aerodynamic potential equation. An unsteady aeroelastic behavior as well as the resultant differential pressure across the surface of a wing can be represented with this solution.

In the DLM, the aerodynamic loads and the vector of downwash are related in the frequency domain as,  $F =$

$$F_a = AIC^{-1}(\omega) w_a \tag{3}$$

where  $AIC(\omega)$  is the matrix of aerodynamic influence at a specific frequency ( $\omega$ ) and  $w_a$  is the downwash vector described in terms of the plate transversal displacement  $W$  and flow velocity  $V$ .

$$w_a = \frac{\partial W}{\partial t} + V \frac{\partial W}{\partial x} \tag{4}$$

The aerodynamic loads and the structural motion are obtained from distinct numerical methods with distinct meshes. Therefore, the transformation matrices are determined using a surface spline scheme in order to interpolate the forces obtained in the doublet-lattice mesh to the nodes of the FE mesh [30]. The resulting displacements of the structural mesh are also interpolated at the corners of the aerodynamic mesh. This way, the aerodynamic forces are,

$$F_w(\omega) = \Phi^T G_{ea} AIC^{-1} \left( \frac{\partial}{\partial t} + V \frac{\partial}{\partial x} \right) G_{ae} \Phi \eta \tag{5}$$

where  $\Phi$  is the modal matrix,  $G_{ea}$  is the aerodynamic to structural transformation matrix and  $G_{ae}$  is the structural to aerodynamics transformation matrix. In this paper, the aerodynamic forces are converted from the frequency domain to the time domain by using the Roger's method [26]. This way, transient and steady state behavior of the system can be investigated. It is important to note that Roger's method uses a minimum square approximation to obtain a rational polynomial formulation described in time domain to represent the aerodynamic forces. Thus, the aerodynamic forces, and subsequently the piezoaeroelastic equations, can be represented in the state-space form,

$$\begin{Bmatrix} \dot{X}_1 \\ \dot{X}_2 \\ \dot{V}_p \\ \dot{X}_s \end{Bmatrix} = \begin{bmatrix} \mathbf{0} & \mathbf{I} & \mathbf{0} & \mathbf{0} \\ -M_s^{-1}(K_s + K_{NL}) & -M_s^{-1}B_s & M_s^{-1}\theta & M_s^{-1}A_j \\ \mathbf{0} & \frac{-\theta^T}{R_L} & -\frac{1}{R_L C_p} & \mathbf{0} \\ \frac{V}{b} \gamma I & \mathbf{0} & \mathbf{0} & \mathbf{I} \end{bmatrix} \begin{Bmatrix} X_1 \\ X_2 \\ V_p \\ X_s \end{Bmatrix} \tag{6}$$

The piezoaeroelastic behavior of the wing is governed by Eq. (6) that is solved by using the alfa-generalized and the Newton Raphson method. The alfa-generalized [31-33] is employed to numerically integrate the system equation in time domain. The equations that describes the alpha generalized method are shown,

$$\dot{x}_{n+\alpha_{nl}} = A^* x_{n+\alpha_{nl}} \tag{7.a}$$

$$x_{n+1} = x_n + h \dot{x}_n + h \gamma_1 (\dot{x}_{n+1} - \dot{x}_n) \tag{7.b}$$

$$\dot{x}_{n+\alpha_{nl}} = \dot{x}_n + \alpha_{nl} (\dot{x}_{n+1} - \dot{x}_n) \tag{7.c}$$

$$x_{n+\alpha_{fl}} = x_n + \alpha_{fl} (\dot{x}_{n+1} - \dot{x}_n) \tag{7.d}$$

where  $A^*$  is the nonlinear state space matrix and  $h$  is the time step. In order to solve the set of nonlinear equations, which describes the piezoaeroelastic generator, the Newton-Raphson method is used. A brief explanation of this method is presented next. In the first time step the state variables are known. As an initial guess, the state variable of the next time step is assumed as the same of the one of the current time step. Later, the residue and Jacobian are calculated in order to update the state by,

$$\Delta \mathbf{x}^k = -\mathbf{J}(\mathbf{x}^k)^{-1} \mathbf{R}(\mathbf{x}^k)$$

where  $\mathbf{R}$  is the residue and  $\mathbf{J}$  the Jacobian. If the norm of the calculated value (Eq. 8) is greater than an assumed value, the state variable vector is updated in the next time step as,

$$\mathbf{x}_{n+1}^{k+1} = \Delta \mathbf{x}_{n+1}^k + \mathbf{x}_{n+1}^k$$

and a new Jacobian, residue and actualization vector are calculated. The norm is again verified and when the norm of the actualization vector is smaller than an assumed value, the time step is changed.

### 3. NONLINEAR ELECTROAEROELASTIC MODEL

This section investigates the nonlinear piezoaeroelastic behavior of cantilevered plate-like wings with embedded piezoceramics. The effect of wing aspect ratio (AR) on the electroaeroelastic behavior (mechanical and electrical outputs) is discussed. Five different aspect ratios (varying from 1 to 5) as well as a set of load resistances (ranging from short circuit to open circuit condition) are considered in the simulations. The linear case is first investigated in this work. By neglecting the nonlinear stiffness term in Eq. (1a), the variation of the linear flutter speed and flutter frequency are obtained for the aspect ratios considered in this work. Later, the nonlinear piezoaeroelastic behavior is investigated (wing tip displacement, voltage and power output) for the different aspect ratios and load resistances.

The geometric properties of the different wings used in the simulations are presented in Table 1. The convergence of the piezoaeroelastic solution (FE model and aerodynamic model) was verified for each AR. The mesh of the basic configuration (AR = 1) is 10x10. The number of elements along the chord is always the same for different AR and the number of elements along the span is increased by 10 for increasing AR.

Table 1- Geometric properties of the generators

Caso	Aspect Ratio	Span [m]	Chord [m]	Thickness [m]
RA1	1	0.3	0.3	0.001
RA2	2	0.6	0.3	0.001
RA3	3	0.9	0.3	0.001
RA4	4	1.2	0.3	0.001
RA5	5	1.5	0.3	0.001

Two identical layers of PZT-5A are embedded into the top and the bottom of the aluminum structure and each one has a thickness of 0.4 mm. These embedded piezoceramics layers cover 0.01 m of the wing span (at the root) in all cases (AR) considered in this work. The geometric and material properties of the plate-like wing are presented in Table 2. The material and electromechanical properties for PZT-5A are given in Table 3. The air density is assumed to be 1.225 kg m<sup>3</sup> and sound speed of 340 m/s.

Table 1- Aluminum mechanical properties

Material	Aluminum
Elastic Modulus	69 GPa
Poisson coefficient	0.3
Density	2750 kg/m <sup>3</sup>

Table 2- Material and electromechanical properties of PZT-5A

Material	PZT 5A
----------	--------

Elastic Modulus	69.5 <i>GPa</i>
Poisson coefficient	0.3
Density	7800 <i>kg/m<sup>3</sup></i>
Dielectric constant ( $\epsilon^s$ )	11.51 <i>F/m</i>
Piezoelectric constant ( $e_{31}$ )	5.2 <i>C/m<sup>2</sup></i>
Piezoceramic thickness	0.4 <i>mm</i>

Although the objective of this article is to investigate the influence of aspect ratio on the nonlinear electroelastic behavior of the wind energy harvester, the linear behavior is first discussed. The undamped natural frequencies and modes sequence are presented in Table 4 and 5. They are obtained by neglecting the nonlinear term in Eq. 1a. The short-circuit condition ( $RL=100 \Omega$ ) is considered. One should note in Table 4 that natural frequencies decrease with increasing AR (for the first five modes).

Table 3 - Undamped natural frequencies for different AR [Hz]

RA1	RA2	RA3	RA4	RA5
9.26	2.23	1.02	0.57	0.36
22.61	9.96	6.33	3.58	2.29
52.65	14.36	6.39	4.63	3.66
71.29	32.09	17.88	10.06	6.43
74.96	39.35	19.83	14.30	11.19

The modes sequence is shown in Table 5. The sequence is changes as the AR is modified. In Table 5, B stands for a bending mode, T stands for a torsion mode and P stands for plate mode.

Table 4- Mode Sequence

RA1	RA2	RA3	RA4	RA5
1B	1F	1F	1F	1F
1T	1F	1T	2F	2F
2F	2F	2F	1T	1T
1P	2T	3F	3F	3F
2T	3F	2T	2T	2T

The linear piezoeorelastic behavior at short circuit condition is presented here in terms of flutter speed and flutter frequency. The flutter speed is obtained by checking real part of the eigenvalue of the linear system equation. The flutter frequency is obtained from the imaginary part of the eigenvalue. Figure 2a shows the variation of flutter speed with increasing AR. The flutter speed decreases with increasing AR. The variation of flutter frequency with AR is shown in Figure 2b. The flutter frequency decreases with increasing AR.

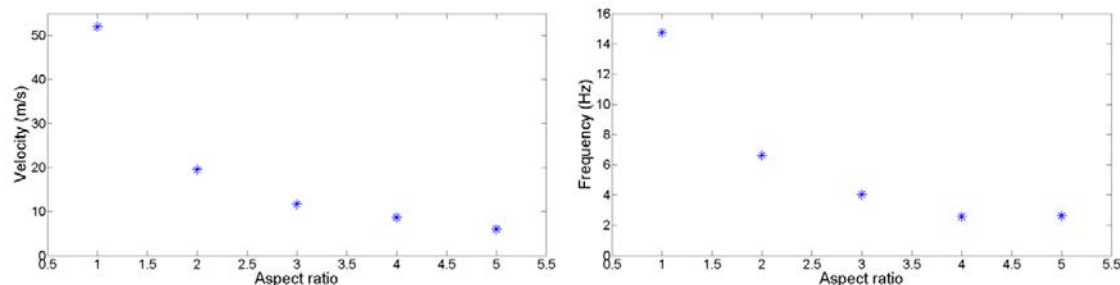


Figure 2 - Flutter speed (a) and flutter frequency (b) versus aspect ratio of the plate.

The nonlinear piezoeorelastic behavior is also investigated and presented as the amplitude of LCOs (tip displacement, voltage output and electrical power output) over a range of airflow speeds for the different AR and load resistances considered in this work. The LCOs are detected in the post flutter region from time domain simulations (FE model and Roger's method for aerodynamics). Figure 3a to 3e show the dimensionless amplitude of LCO for aspect ratios from 1 to 5, respectively. Again, the cut-in speed of LCOs is reduced with increasing AR (but always larger than the linear flutter speed of each case). Also, the range of airflow speeds with LCO of acceptable amplitude is narrowed with increasing AR. For any load resistance, the amplitude increases with increasing airflow speed. The effect of power

generation (using different load resistances) on the vibration amplitude is negligible for all cases. For the case of  $AR = 1$ , the cut-in speed of LCO increases when the load resistance is increased from  $100 \Omega$  to  $1 \text{ k}\Omega$ . For any airflow speed (larger than the cut-in speed) of this same  $AR$ , the mechanical amplitude decreases when the load resistance is increased from  $100\Omega$  to  $1 \text{ k}\Omega$ . For aspect ratios from 2 to 5, the effect of power generation on the mechanical amplitudes is negligible.

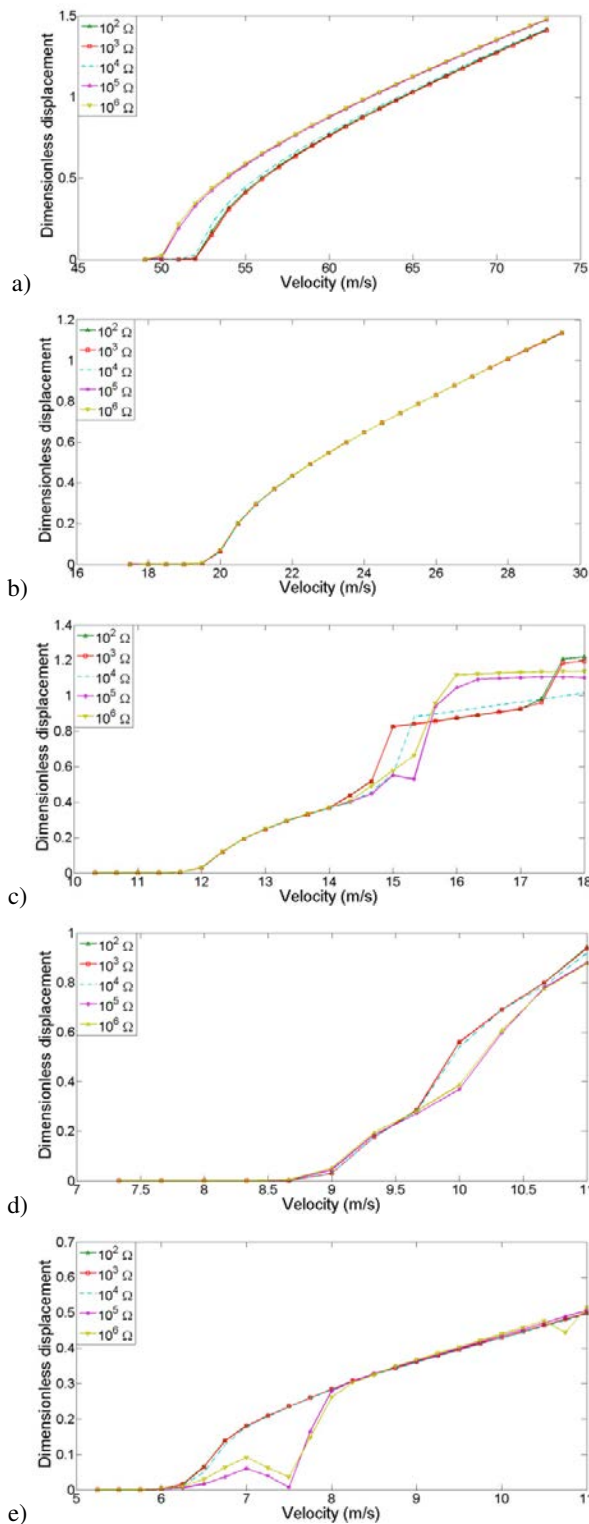
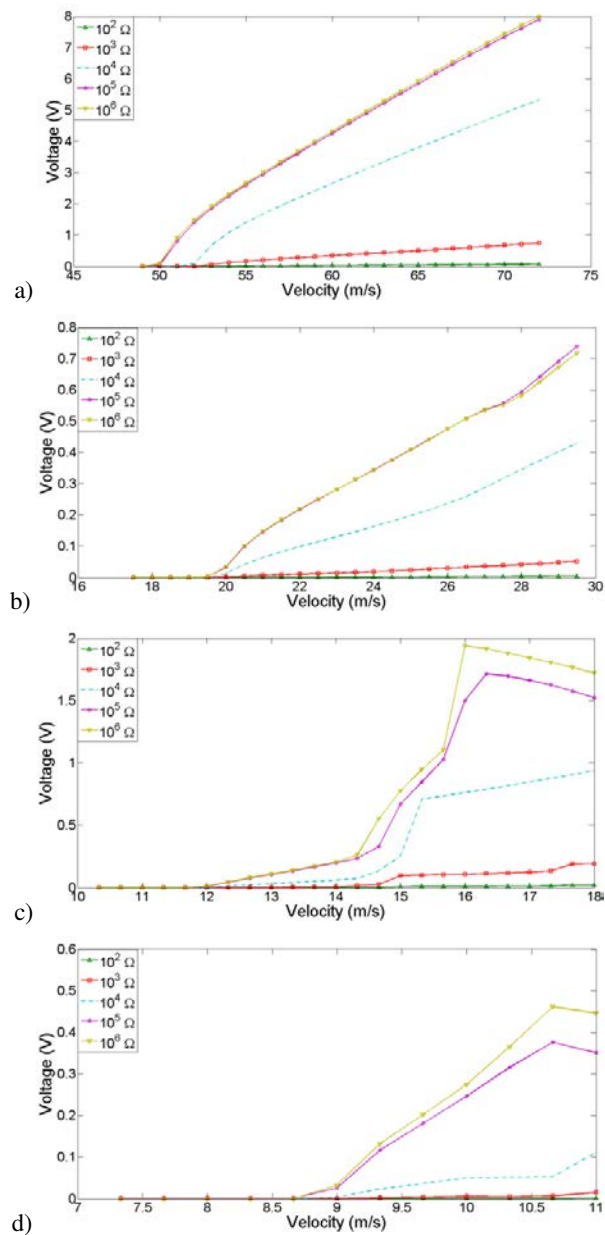
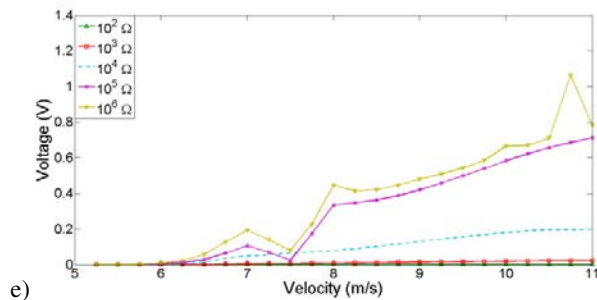


Figure 3 - Dimensionless displacement with increasing airflow speed for five different aspect ratios and a set of load resistances.

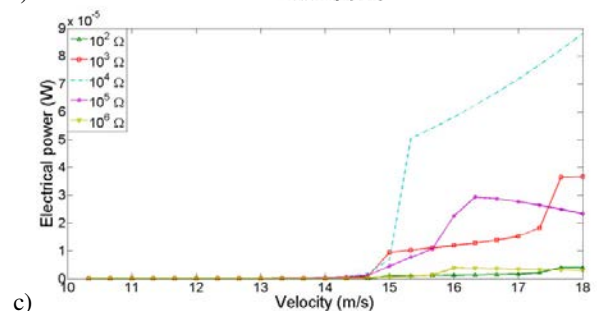
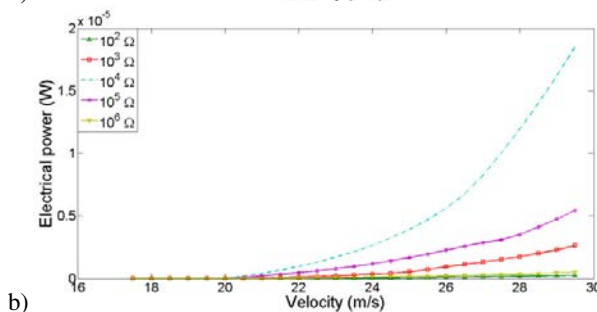
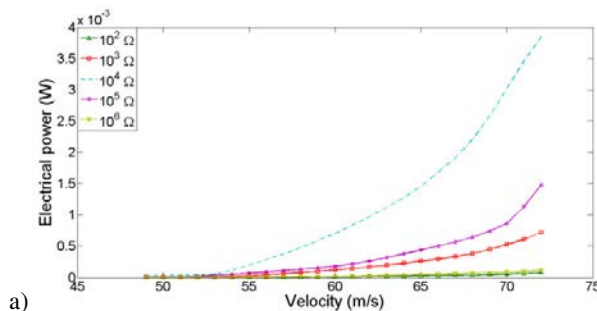
Figure 4a to 4e show the voltage output for aspect ratios 1 to 5, respectively. In general, one should note in Figures 3 that the cut-in speed of LCOs is reduced with increasing AR (but always larger than the linear flutter speed of each case). Also, the range of airflow speeds with LCO of acceptable amplitude is narrowed with increasing AR. The voltage output also decreases with increasing AR. For each AR considered, the voltage output increases with increasing load resistance as well as with increasing airflow speed. Figure 3a (AR = 1) shows that the cut-in speed of LCO increases when the load resistance  $10\text{ k}\Omega$  is used. However, the same cut-in speed is observed for different load resistances when larger aspect ratios are considered (Figs. 3b-e).





e) Figure 4 - Voltage output with increasing airflow speed for five different aspect ratios and a set of load resistances.

Figure 5a to 5e show the power output for the aspect ratios 1 to 5, respectively. In general, one should note in Figures 5 that the cut-in speed of LCOs is reduced with increasing AR (but always larger than the linear flutter speed of each case). Also, the range of airflow speeds with LCO of acceptable amplitude is narrowed with increasing AR. Power output increases with increasing airflow speed for any load resistance and for any aspect ratio. For any aspect ratio (except for AR = 5) and at any airflow speed (larger than the cut-in speed of LCO of each configuration), as the load resistance is increased from 100 Ω to 10 kΩ, the power output increases. When the value of load resistance is further increased, the power output starts decreasing. Therefore, RL =10 kΩ gives the maximum power output among the resistive loads considered for aspect ratios from 1 to 4. This load resistance also gives the largest cut-in speed of LCO when AR = 1. The optimum load for aspect ratio 5 is RL=100 kΩ. One should also note in Figures 4 that maximum power is obtained for AR = 1. Although power decreases with increasing AR, the cut-in speed of LCO also decreases with increasing AR.



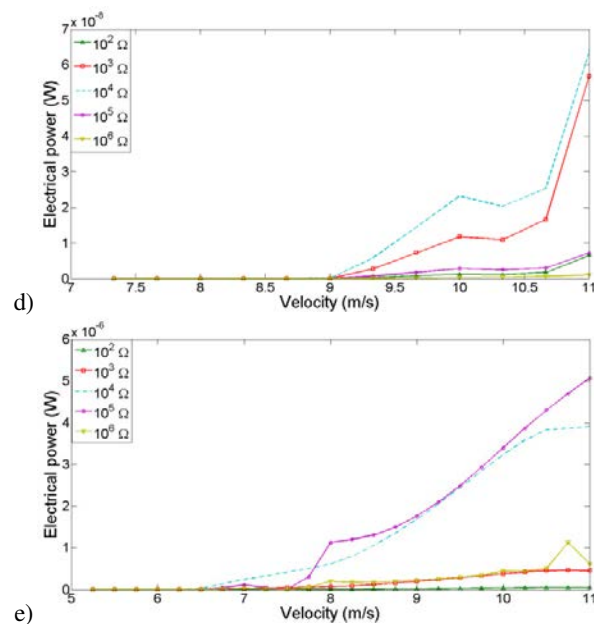


Figure 5 - Power output with increasing airflow speed for five different aspect ratios and a set of load resistances.

#### 4. CONCLUSIONS

In this work, the modeling and analysis of a nonlinear wind energy harvester is presented. The piezoaeroelastic model is obtained by combining a nonlinear electromechanically finite element model, based on the Von Karman plate theory, and an unsteady aerodynamic model based on the DLM method. The aerodynamics is converted to the time-domain by using the Roger's method. The resulting nonlinear equations are integrated numerically using the alpha-generalized method and solved using the Newton-Raphson method.

The linear behavior is first investigated by neglecting the nonlinear stiffness in the governing equations. The effect of aspect ratio on the flutter speed as well as on the flutter frequency is investigated. Five aspect ratios, varying from one to five, are considered. The linear flutter speed and the flutter frequency decrease with increasing aspect ratio.

The nonlinear electroaeroelastic behavior is also investigated for the five aspect ratios considered in the linear case. The cut-in speed of LCO decreases with increasing aspect ratio (although it is always larger than the linear flutter speed of each case). The range of airflow speeds with LCOs of acceptable response amplitude is also decreased with increasing aspect ratio. However, the mechanical and electrical output decrease with increasing aspect ratio (as airflow speed and consequently aerodynamic loads decrease with increasing aspect ratio). In general, the effect of power generation on the mechanical amplitudes is negligible in the nonlinear case.

#### 5. ACKNOWLEDGMENTS

The authors gratefully acknowledge FAPESP (2011/05417-1) for partially funding the present research. The authors also gratefully acknowledge and CNPq and FAPEMIG (558646/2010-7) for partially funding the present research.

#### 6. REFERENCES

- [1] Beeby, S.P., Tudor, M.J. and White, N.M. 2006, "Energy Harvesting Vibration Sources for Microsystems Applications," *Measurement Science and Technology*, Vol. 13, pp. R175-R195.
- [2] Sodano, H.A., Inman, D.J. and Park, G. 2004, "A Review of Power Harvesting from Vibration Using Piezoelectric Materials," *The Shock and Vibration Digest*, Vol. 36, pp. 197-205.
- [3] Anton, S.R. and Sodano, H.A. 2007, "A Review of Power Harvesting Using Piezoelectric Materials 2003-2006," *Smart Materials and Structures*, Vol. 16, pp. R1-R21.
- [4] Priya, S, 2007, "Advances in Energy Harvesting using Low Profile Piezoelectric Transducers," *Journal of Electroceramics*, Vol.19, pp. 167-184.

Vieira, W., De Marqui Jr.  
Modeling and Analysis of a Nonlinear Piezoaeroelastic Wing

- [5] Cook-Chennault, K.A., Thambi, N. and Sastry, A.M., 2008, "Powering MEMS Portable Devices- a Review of Nonregenerative and Regenerative Power Supply Systems with Emphasis on Piezoelectric Energy Harvesting Systems," *Smart Materials and Structures*, 17:043001.
- [6] Erturk, A., Bilgen, O., Fontenille, M., and Inman, D.J., 2008, "Piezoelectric Energy Harvesting from Macro-Fiber Composites with an Application to Morphing Wing Aircrafts," *Proceedings on the 19th International Conference of Adaptive Structures and Technologies*, Monte Verità, Ascona, Switzerland, 6-9 October 2008.
- [7] De Marqui, Jr., C., Erturk, A., and Inman, D. J., 2010a, "Piezoaeroelastic Modeling and Analysis of a Generator Wing with Continuous and Segmented Electrodes," *Journal of Intelligent Material Systems and Structures*, Vol. 21, No. 10, pp.983-993.
- [8] De Marqui, Jr., C., Vieira, W.G.R., Erturk, A., and Inman, D. J., 2010b, "Modeling and Analysis of Piezoelectric Energy Harvesting from Aeroelastic Vibrations Using the DoubletLattice Method, *Journal of Vibration and Acoustics*, in Vol. 133, pp. 011003-1 – 011003-9
- [9] Bisplinghoff, R. L. and Ashley, H., 1962, *Principles of Aeroelasticity*, John Wiley and Sons, NY.
- [10] Fung, Y. C., 1969, *Introduction to the Theory of Aeroelasticity*, Dover Publications
- [11] Dowell, E. H., Curtiss, H. C., Jr., Scalan, R. H., Sisto, F., 1978, *A Modern Course in Aeroelasticity*, Sijthoff and Norrdhoff, the Netherlands.
- [12] Hodges, D.H. and Pierce, G.A., 2002, *Introduction to Structural Dynamics and Aeroelasticity*, Cambridge University Press, New York.
- [13] Bryant, M. and Garcia, E., 2009, Development of an Aeroelastic Vibration Power Harvester, *Proceedings of SPIE* 7288, 728812.
- [14] Bryant, M. and Garcia, E., 2009, Energy Harvesting: A Key to Wireless Sensor Nodes, *Proceedings of SPIE* 7493, 74931W.
- [15] Peters, D. A., Karunamoorthy, S., Cao, W. M., 1995, Finite State Induced Flow Models; Part I; Two Dimensional Thin Airfoil, *Journal of Aircraft*, 32, pp. 313-322.
- [16] Erturk, A., Vieira, W.G.R, De Marqui, Jr., C. and Inman, D.J., 2010, On the Energy Harvesting Potential of Piezoaeroelastic Systems, *Applied Physics Letters*, 96, 184103.
- [17] Theodorsen, T., 1935, *General Theory of Aerodynamic Instability and Mechanism of Flutter*, Langley Memorial Aeronautical Laboratory, NACA-TR-496.
- [18] McKinney, W. and DeLaurier, J.D., 1981, The Wingmill: An Oscillating-Wing Windmill, *Journal of Energy*, 5, pp.109–115.
- [19] Ly, K.H. and Chasteau, V.A.L., 1981, Experiments on an Oscillating-Wing Aerofoil and Application to Wing-Energy Converters, *Journal of Energy*, 5, pp. 116–121.
- [20] Jones, K.D. and Platzer, M.F., 1999, Oscillating-Wing Power Generator, *Proceedings of ASME/JSME-Joint Fluids Engineering Conference*, No. 7050.
- [21] Nayfeh, A.H. and Mook, D.T., 1979, *Nonlinear Oscillations*, John Wiley and Sons, New York.
- [22] Moon, F.C., 1987, *Chaotic Vibrations*, John Wiley and Sons, New York.
- [23] Dowell, E.H., Edwards, J. and Strganac, T., 2003, Nonlinear Aeroelasticity, *AIAA Journal of Aircraft* 40, 857-874.
- [24] Abdelkefi, A., Nayfeh, A.H., Hajj, M.R., 2011, Modeling and Analysis of Piezoaeroelastic Energy Harvesters, *Nonlinear Dynamics*, 67, 925-939.
- [25] Sousa, V.C., Anicézio, M.M., De Marqui, Jr., C., and Erturk, A., 2011, Enhanced Aeroelastic Energy Harvesting by Exploiting Combined Nonlinearities: Theory and Experiment, *Smart Materials and Structures*, 20, 094007.
- [26] Roger, K. L., 1977, Airplane Math Modeling Methods for Active Control Design, *AGARD-CP-228*, p. 4.1-4.11.
- [27] Reddy J. N. *Mechanics of Laminated Composite Plates and Shells. Theory and Analysis* (2nd edn). CRC Press: Boca Raton, FL, 2004.
- [28] Lee, Y.Y., Sun, H. Y., Reddy, J.N., 2005, Non-linear Finite Element Modal Approach for the Large Amplitude Free Vibration of Symmetric and Unsymmetric Composite Plates, *International Journal for Numerical Methods in Engineering*, 65, 45-61.
- [29] Albano, E., and Rodden, W. P., 1969, "A Doublet-Lattice Method for Calculating Lift Distributions on Oscillating Surfaces in Subsonic Flow," *AIAA J.*, 7, pp. 279–285.
- [30] Harder, R. L., and Desmarais, R. N., 1972, "Interpolation Using Surface Splines," *Journal of Aircraft*, 9, pp. 189–191.
- [31] Chung, J., Hulbert, G.M., , "A Time Integration Algorithm for Structural Dynamics with Improved Numerical Dissipation: The Generalized- $\alpha$  Method", *Journal of Applied Mechanics* , (1993) Vol60, pp. 371-375.
- [32] Shearer, C.M., Cesnik, C.E.S., "Modified Generalized- $\alpha$  for integrating governing equations of very flexible aircraft", 47th AIAA/ASME/ASCE/AHS/ASC Structures, Structural Dynamics and Materials Conference, AIAA Paper 2006-1747, 2006.
- [33] Shearer, C.M., Cesnik, C.E.S., "Nonlinear Flight Dynamics of Very flexible Aircraft", *Journal of Aircraft*, Vol. 44, No 5, September-October 2007

## 7. RESPONSIBILITY NOTICE

22nd International Congress of Mechanical Engineering (COBEM 2013)  
November 3-7, 2013, Ribeirão Preto, SP, Brazil

The authors are the only responsible for the printed material included in this paper.